

Unveiling the early stage evolution of local atomic structures in the crystallization process of a metallic glass

Lin Ma (马琳)^{1*}, Xiao-Dong Yang (杨晓东)^{1*}, Feng Yang (杨锋)¹,
Xin-Jia Zhou (周鑫嘉)¹, Zhen-Wei Wu (武振伟)^{1†}

¹Institute of Nonequilibrium Systems, School of Systems Science, Beijing Normal University,
100875 Beijing, China

February 5, 2024

Abstract

The early stage evolution of local atomic structures in a multicomponent metallic glass during its crystallization process has been investigated via molecular dynamics simulation. It is found that the initial thermal stability and earliest stage evolution of the local atomic clusters show no strong correlation with their initial short-range orders, and this leads to an observation of a novel symmetry convergence phenomenon, which can be understood as an atomic structure manifestation of the ergodicity. Furthermore, in our system we have quantitatively proved that the crucial factor for the thermal stability against crystallization exhibited by the metallic glass, is not the total amount of icosahedral clusters, but the degree of global connectivity among them.

Keywords: metallic glass, crystallization, molecular dynamics simulation, local atomic clusters

PACS: 64.70.pe, 68.55.A-, 64.60.aq

1. Introduction

Since the advents of multicomponent metallic glasses (MGs) in the early 1990s, the initial atomic-scale structure evolution and nanocrystallization under annealing or mechanical loading treatments of their glass-forming liquids, have been extensively investigated for both fundamental and practical reasons [1–21]. Various unique internal structures of MGs underlie their interesting properties, which render MGs potentially useful for distinct applications [22–25]. For the excellent mechanical properties of glasses with nanocrystalline inclusions and as well fundamental meanings to solid state physics, numerous studies have been conducted to comprehend how amorphous alloys crystallize at nanoscales. However, due to the lack of directly time-resolved data of atomic structure evolutions at the early stage of crystallization, clear pictures of how localized atomic structures rearranging themselves, developing original translational symmetry, and eventually forming nanocrystals with three-dimensional (3-D) periodicity, remain less well-understood at present. Especially the questions that which

*These two authors contribute equally to this work.

†Corresponding author Email: zwwu@bnu.edu.cn

local parts of the MGs will the firstly get into the structure with embryonic translational symmetry, what kind of features these local parts have, and how they will evolve in the future, are still mysterious at present.

Through high-resolution transmission electron microscopy (HRTEM) and advanced structural analysis techniques, researchers have accumulated massive precious experimental data to study and reveal the MGs' structure evolution under certain treatments^[4–6,10,11]. A series of meaningful achievements have been obtained. But HRTEM cannot give us the answers of these problems mentioned above. A clearly physical picture that can describe the details of the evolutions associated with different atomic-scale structures and the features of these localized structures has not been obtained now. The quantitative description of this process is still in its early stages.

The icosahedral short-range order (ISRO) in MGs is generally adopted as a structural indicator for the fundamental process underlying structural relaxation^[26–29]. However, in some MGs the ISRO is absent. As shown in Ref. [30], atomic symmetry is a more general concept in the glass-forming alloys in which both local fivefold and translational symmetries are present. Both experimental and simulated researches have shown that local clusters symmetry plays an important role in determining many properties of MGs. Therefore, it is worth to check that whether the degrees of the local fivefold symmetry (LFFS) and the local translational symmetry (LTS) connected with the analysis of local icosahedral clusters, especially the spatial topological order of them, are more crucial for the understanding of the structural evolution and thermal stability of MGs.

In this study, to address above challenges we performed molecular dynamics (MD) simulation with the LAMMPS code^[31], and the degrees of LFFS and LTS were used as the structural indicators to identify and characterize the irreversible structural evolutions in the crystallization process. The spatial correlation of the icosahedral clusters in the glass structures and its influence on the thermal stability of MGs against crystallization has also been investigated. We find that the initial stability and the very beginning evolution of the local atomic structure are basically unaffected by the degree of LFFS of these regions. Moreover, it is found that not the quantity of the icosahedral clusters but the connectivity among them, will be the crucial factor for the thermal stability against crystallization in amorphous alloys.

2. Methodology

In our MD simulations, a model system of $\text{Zr}_{65}\text{Al}_{30}\text{Cu}_5$ containing 10000 atoms in a cubic box with periodic boundary conditions was adopted. The realistic embedded-atom method potential used is the one developed based on the data in Ref. [32]. The integration time step of all simulations was set to 2 fs. In the process of sample preparation, it was first melted and equilibrated at $T = 2500\text{K}$ for 1 ns, and then cooled down to 290K with a cooling rate of 10^{12}K/s (10^{13}K/s), during which the cell size was adjusted to maintain zero pressure in the NPT ensemble. Finally, the sample was relaxed at 290K for another 1 ns. To ensure the reliability of the MD-generated atomic configurations, the pair correlation functions (PCFs) of the model were calculated to declare the amorphous states of the samples. For investigating the crystallization process, annealing treatment was applied on the sample at $T = 650\text{K}$ (above the kinetic glass transition temperature $T_g = 615\text{K}$) in the NPT ensemble for doing the following analysis.

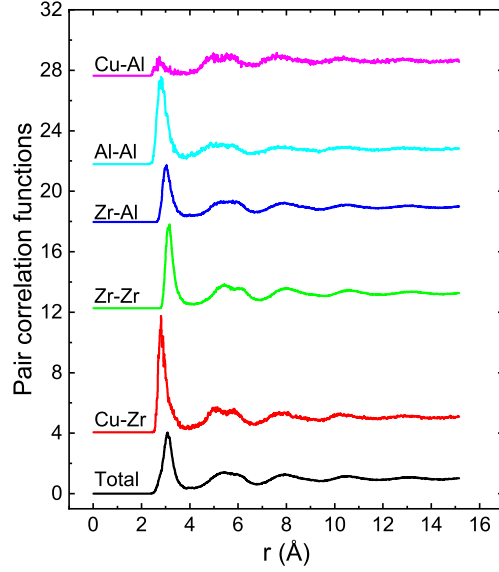


Fig. 1. (color online) The calculated PCFs of the MD-generated atomic configurations obtained at a cooling rate of 10^{13} K/s. For clarity, the noisy and scattered Cu-Cu partial PCF is not included.

3. Results and Discussion

The PCFs of the amorphous $\text{Zr}_{65}\text{Al}_{30}\text{Cu}_5$ alloy obtained through MD simulation are presented in Fig. 1. The overall PCF exhibits a shoulder on the second peak, and the Zr-Zr partial PCF displays the largest distance for the first peak, consistent with the previous experimental findings on these alloys [33]. Additionally, the Cu-Zr and Zr-Zr partial PCFs show a characteristic splitting of the second peak into two subpeaks, which is a common feature observed for metallic glasses [34]. These results, to some extent, affirm the reliability of the MD-generated atomic configurations for the subsequent analysis. Figure 2(a) presents the potential energy (PE) evolution of the entire system as a function of scaled-time during the isothermal annealing process. The onset of crystallization is evident by the PEs exhibiting a drop at a scaled-time of $0.5 \sim 0.6$. This decrease signifies the initiation of crystallization. Notably, Figure 2(a) also illustrates distinct variation trends in the PEs of two samples generated with different cooling rates. It is worth to note that we do not emphasise the relationship between the rate of cooling and the rate of crystallization here. The two different cooling rates were used to produce two different configurations for the subsequent analysis. In other words, the only purpose here choosing two slightly different cooling rates is to generate two samples that are similar in short-range orders but with a bit subtle difference in medium-range orders (as it can be seen below). And we also performed the iso-configurational runs to take the thermal fluctuation effect into account. It was found that only ~ 8 cases out of 40 that the fast-quenched sample took much longer time to crystallize than the slow-quenched one, and the *simply* isoconfigurational averaged crystallization-time (in practical defined as the middle-term of the PE's drops) of the slow-quenched sample is 3.6ns which is indeed statistically longer than the one of fast-quenched sample's 2.8ns. More impressively, as it can be seen in Fig. 2(b), the distribution of the crystallization-time for the slow-quenched sample is bimodal, in which there is a peak (This peak remains after increasing the statistical sample size to 80, ruling out the possibility that this is a statistical rise and fall.) located at long-time intervals, what is significantly different from the one of the fast-quenched samples. Apparently, all above results indicate

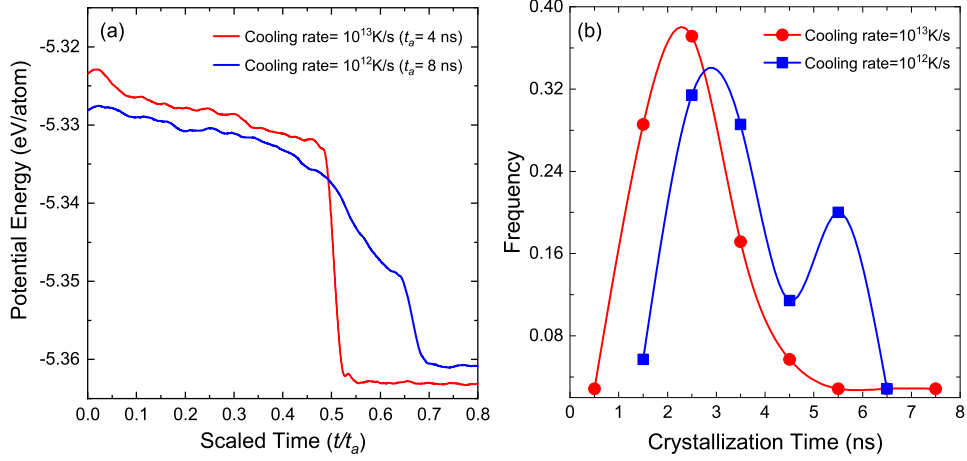


Fig. 2. (color online) (a) The annealing time dependence of the system potential energy during the isothermal annealing treatment at 650K. For clarity, the time is scaled by t_a which is the total annealing time for the two samples respectively. (b) The distribution of isoconfigurational averaged crystallization-time.

that the initial atomic structure indeed plays an important role on the thermal stability of our metallic liquid. The underlying reasons for this intriguing phenomenon will be further explored in subsequent sections of this work.

The atomic structure changes throughout the annealing process are indicated by the temporal evolution of the PEs, as demonstrated by the evolving PCFs in Fig. 3, which illustrate a transition from an amorphous state to a crystalline solid. To comprehensively investigate the local structural rearrangement preceding crystallization, we employed the Voronoi tessellation analysis^[35,36]. This method involves dividing the three-dimensional space into cells centered around each atom. A plane is drawn to bisect each line connecting the central atom and its nearest-neighbors, resulting in the formation of a Voronoi cell enclosed by these inner planes. The Voronoi index $\langle n_3, n_4, n_5, n_6 \rangle$ is utilized to characterize the atomic clusters surrounding each atom, where n_i represents the number of i -edged faces of the corresponding Voronoi cell. The presence of an i -edged face reflects the local symmetry of the central atom with its nearest neighbors in a specific direction. Notably, faces with three, four, and six edges exhibit LTS features, while pentagon faces indicate the presence of LFFS. The degree of LFFS in local structures is quantified using a specific metric defined as $d_5 = n_5 / \sum_i n_i$ ^[30]. Additionally, by analyzing the coordination information of atoms obtained from the Voronoi analysis, the system's global bond-angle distributions can be measured. We selected a number of different annealing time periods and analyzed the local structures of the corresponding atomic configurations. The results shown in Fig. 4 reveal the changes in bond angle distributions, which demonstrate a gradual increase in LTS features within the system throughout annealing. The initial bond angle distribution clearly indicates the amorphous state of the sample. As the annealing process progresses, characteristic angles of 90° , 120° , and 180° gradually emerge and become more prominent, suggesting an enhancement of ordering in the system. The variation in the fraction of i -edged faces in the Voronoi polyhedrons (Fig. 4) also supports the aforementioned trend. The evolution of these local symmetries behaves similarly in the samples with different cooling rates, despite the fact that the sample generated with a lower cooling rate evolves more gradually while the one generated with a higher cooling rate crystallizes more suddenly after a bit gentle embryo state processing. Below we will discuss this behavior in

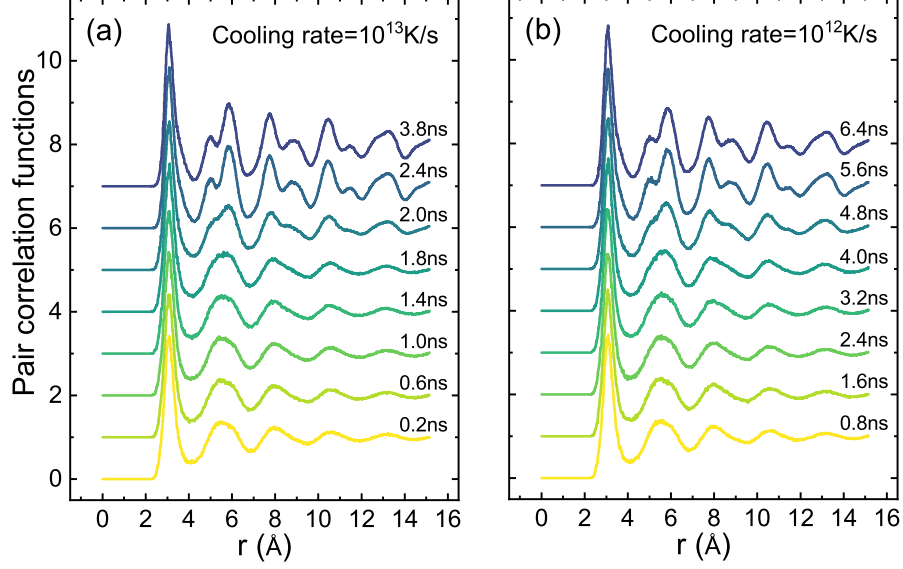


Fig. 3. (color online) Changes in the total PCFs during the crystallization of two MG samples obtained at different cooling rates. (a) Cooling rate = 10^{13} K/s. (b) Cooling rate = 10^{12} K/s.

more details.

To provide a detailed description of the evolution of local structures with different symmetry characteristics, we used the degree of LFFS d_5 in Voronoi cells associated with local atomic clusters to label corresponding regions and then examine the subsequent variation of d_5 of these regions in the annealing process. As shown in Fig. 5, in contrast to some previous observations where regions with a higher degree of LFFS exhibited greater stability, and regions with lower degree of LFFS underwent more frequent irreversible rearrangements, our results indicate that the thermal stability and evolution speed of local structures are basically unaffected by the degree of d_5 of these regions during annealing. Notably, we observed a phenomenon of symmetry convergence (Fig. 5), where local structures with different initial LFFS characteristics undergo transformations in their localized environments, leading the entire system towards a state where the degree of LFFS is approximately 0.4. After this convergence phenomenon, d_5 begins to fall fast, indicating that the system is crystallising, the growth and development of nanocrystals occur randomly within the samples. Based on the aforementioned discussion, our aim is to elucidate the key mechanism behind the nucleation of high-density nanosized crystals during the initial stages of crystallization in MGs under supercooled liquid conditions^[6,7,37–39]. We propose that the convergence of local structure symmetry results in the system transitioning into an embryo stage, a process that can be understood as the atomic-structure manifestation of ergodicity, which makes sure that every local region in the sample has the potential to nucleate and grow into crystals from a liquid state. To further substantiate our viewpoints, we provide a more detailed description of the evolution of local atomic structures with dissimilar symmetries. Utilizing a sample with a cooling rate of 10^{13} K/s, we employ the degree of d_5 to label different local atomic regions. In addition to examining the variation in d_5 for the corresponding atomic clusters, we also investigate the changes in triangular ($d_3 = n_3 / \sum_i n_i$), quadrilateral ($d_4 = n_4 / \sum_i n_i$), and hexagonal faces ($d_6 = n_6 / \sum_i n_i$) with LTS features during the evolution process (Fig. 6). The results further confirm that the thermal stability and earliest evolution of atomic clusters are not correlated with their original local symmetries.

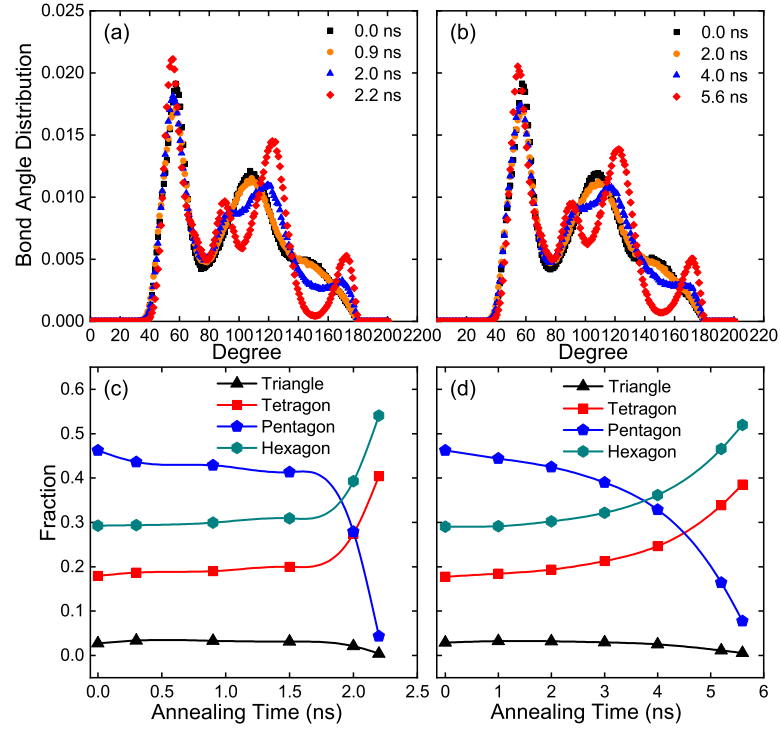


Fig. 4. (color online) The variations of the bond-angle distributions and degree of LFFS and LTS of the MGs system during the annealing process. (Cooling rate= 10^{13} K/s, in (a) and (c); cooling rate= 10^{12} K/s, in (b) and (d).)

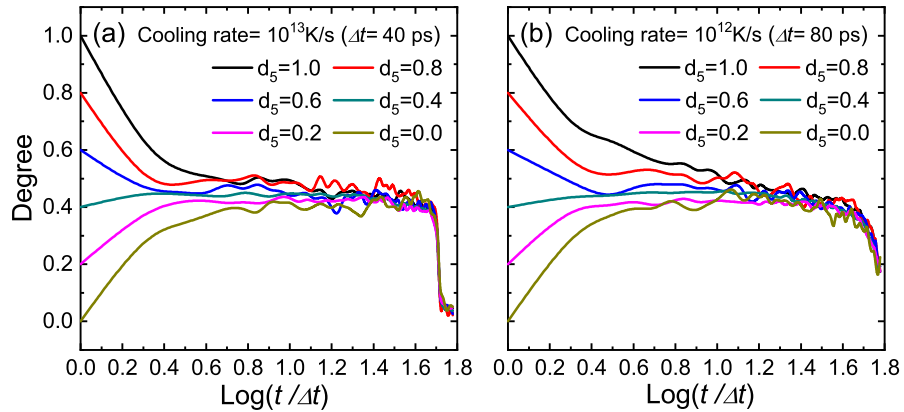


Fig. 5. (color online) The evolution of d_5 of different local atomic regions classified by their corresponding original degree of d_5 (from 0.0 to 1.0) for the samples with two different cooling rate during the annealing process. (a) Cooling rate= 10^{13} K/s. (b) Cooling rate= 10^{12} K/s. Δt is the configuration sampling time interval.

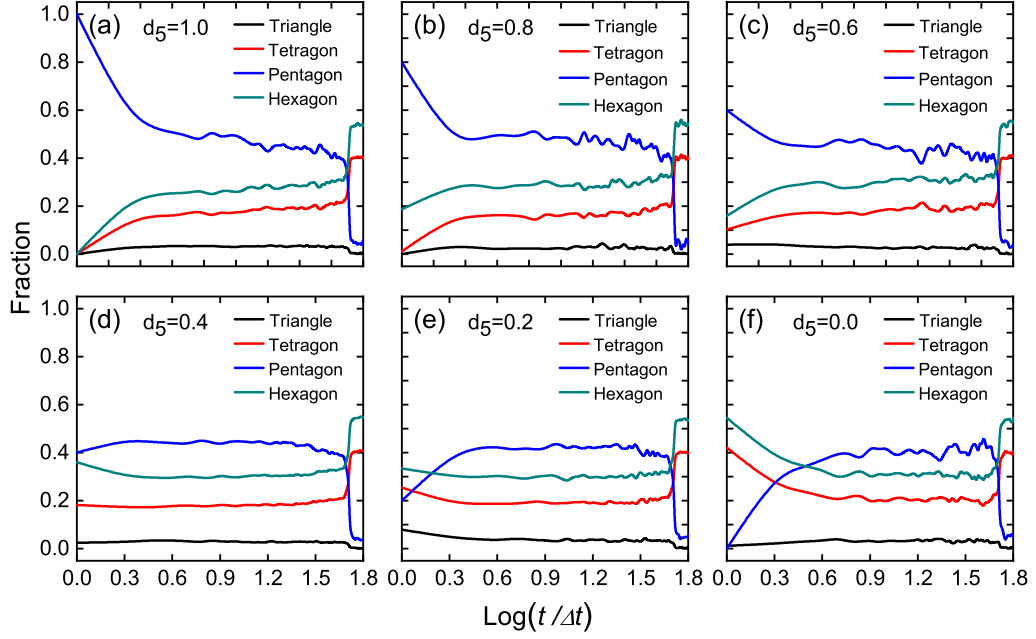


Fig. 6. (color online) The change of d_3 , d_4 , d_6 , and d_5 of different local atomic regions classified by their corresponding original degree of d_5 ((a) $d_5 = 1.0$, (b) $d_5 = 0.8$, (c) $d_5 = 0.6$, (d) $d_5 = 0.4$, (e) $d_5 = 0.2$, (f) $d_5 = 0.0$.) for the sample with a cooling rate of 10^{13} K/s during the annealing process. The time interval Δt on the x-axis corresponds to 40 ps.

After elucidating the initial-stage evolution of the local atomic clusters, our focus now shifts to understanding the factors behind the disparate changes observed in the PE curves which correspond to the differences in thermal stability of samples produced at different cooling rates. Figure 7(a) presents the average fraction of pentagonal faces, reflecting the LFFS of the entire system, along with the presence of triangular, quadrilateral, and hexagonal faces exhibiting the LTS features. The result suggests that the different cooling rates we considered here have a negligible impact on the prevalence of both LFFS and LTS in the corresponding samples. As well, the proportions of icosahedral clusters $\langle 0, 0, 12, 0 \rangle$ in the two as-quenched samples, as well as their variations during the annealing process were shown in Fig. 7(b). The results unequivocally demonstrate that, despite the similar initial fractions of $\langle 0, 0, 12, 0 \rangle$ in these two samples generated at different cooling rates, their subsequent evolution over time exhibits substantial disparity. Consequently, we naturally infer that the underlying mechanism accounting for the aforementioned diversity lies in the distinctive packing and correlation of icosahedral clusters within the glass structures. This investigation addresses a crucial question regarding the connectivity and arrangement of local icosahedral clusters, which profoundly influence the thermal stability and crystallization process in these two samples.

To investigate the network and extended clusters (ECs) formed by the interconnection of the $\langle 0, 0, 12, 0 \rangle$ clusters, here we introduced the method of graph theory approach. The central atoms of all icosahedral clusters will be treated as nodes in a network, and if two different central atoms have the same one atom as their common nearest-neighbors, the two represented nodes are considered to be connected. The number of the sharing atoms will be used as the weight of this link. Now the question is transformed into a mathematical problem, obtaining and analyzing the connected components (i.e. the ECs in the glass structures) in a graph. The connectivity number (N_{con}) which characterizes the space length scales of ECs is defined as the number

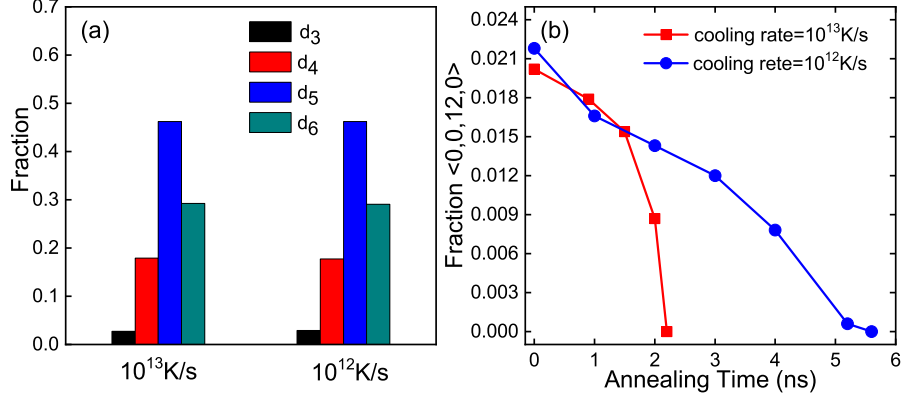


Fig. 7. (color online) (a) The fractions of i-edged faces in polyhedra of two samples associated with different cooling rates. (b) The variation of the fractions of the icosahedral clusters during the isothermal annealing treatment.

of nodes in a connected component in the corresponding graph. Distributions of N_{con} at several time points during the isothermal annealing process have been shown in Fig. 8. It can be seen that the icosahedral clusters in the samples generated under a lower cooling rate exhibit stronger spatial correlations, and they tend to be connected with each other. The results indicate that the low cooling rate will enhance the spatial correlations of the icosahedral clusters and consequently increase the stability of the ECs network in the sample, which would be the key factor of dynamic slowing down to prevent the crystallization. In order to make different dimensional ECs have comparability, we define strength factor for an EC as $\sum w_i/N_{con}$, where N_{con} is the number of nodes in an EC, and w_i is the sum of weight of all links in this connected component abstracted for the corresponding EC. The global strength factor of the network representing the atomic structure will be defined as the sum of the strength factors over all ECs. The outcome implies that the two adopted cooling rates lead to small difference (about 7.3%, see Fig. 7) in the quantity of icosahedral clusters in two samples, but large influence (about 27.4%, see Fig. 8) on the global strength factor of the samples. The results demonstrate once more that the thermal stability against crystallization do not depend on the total quantity of the icosahedral clusters, but on the degree of connectivity among them in our cases. As well, the variation of the system strength factor also has been given in Fig. 8. It can be seen that systems subjected to different cooling rates exhibit distinct evolving behavior during the crystallization process, which indicates that the system strength factor is a good indicator for the thermal stability of the MGs and strongly correlated with the evolutionary time-scales in the crystallization process of them. And this also can be used to rationalize what we found in Fig. 2(b), the bimodal feature, by the fact that in the slow-quenched samples the stochastic nucleus's development and the subsequent crystal growth will be greatly influenced by how close it is to a compact extended icosahedral-clusters, where the connectivity strength is relatively high.

The crystallization is a complex physical process consisting of two major events, nucleation and crystal growth which are driven by thermodynamic, chemical, dynamic, as well as local structure properties. It has been well documented in the literatures that the presence of icosahedral clusters and of connected icosahedra plays an important role on the dynamic slowing-down of the metallic liquids during supercooling^[14,27]. Therefore, what we found here can be attributed to the fact that a more compact icosahedral network will stabilize the dynamics of the liquids a bit and then hinders the crystal growth process. At the same time, even more interesting and

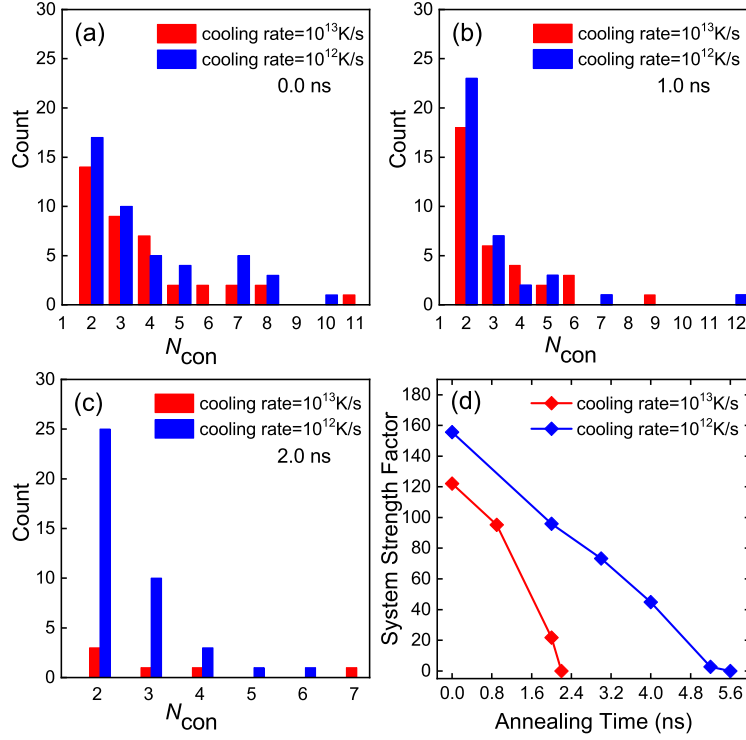


Fig. 8. (color online) The distributions of N_{con} at several time points ((a)0.0 ns, (b)1.0 ns, (c)2.0 ns.) during the isothermal annealing process. (d) The change in system strength factors of two samples with dissimilar cooling rate during the isothermal annealing process.

complicated, the presence of the icosahedra network possessing lower formation energy^[40] could also increase the free energy barrier of the nucleation process in the view of it makes the interface between the crystal nuclei and the surrounding medium a bit rough (effectively large interface area), which leads to a potentially more interface free energy cost and then against the crystallization^[41,42]. In other words, the increase of crystalline embryos and the decrease of icosahedral connectivity during annealing seem to imply that there is a mutual constraint between the two factors. On the one hand, with the growth of crystalline embryos, the connectivity of icosahedra is damaged, which drives the whole crystallization process; on the other hand, the connectivity of icosahedral clusters inhibits the formation of crystalline embryos. Especially when a much slower cooling rate was adopted, the crystal-like short-range orders may start to organize to form some extended structures, which would definitely influence the following crystallization process when the sample was annealed at some temperatures. The interplay between the embryos of crystallization and the connectivity of icosahedra on the thermal stability of the liquid will become even more complicated at that time^[42,43], and the mechanism of the interaction between these two factors in the metallic glass-forming systems is a thought-provoking issue that deserves an in-depth investigation in the future.

4. Conclusion

In this study, we provided a refined description of the evolutionary details of the atomic structures with different local symmetries in the crystallization process of a metallic glass. At the very beginning of the de-

vitriification, the results suggest that the thermal stability and the earliest atomic structure evolution have no correlation with their short-range order (SRO) characters, which leads to a novel phenomenon of local symmetry convergence being found. We propose that this could be the key mechanism for the nucleation of high-density nanocrystals at the beginning of the crystallization process of MGs under the deep supercooled conditions^[6,7,37–39]. Furthermore, it has been clarified that in our system the thermal stability against crystallization does not depend on the total amount of the icosahedral SRO, but on the degree of global connectivity among them, which is a result might promote future studies of the theory for nucleation and growth of crystals in the disordered systems. At last, it is worth to note that the global strength factor which quantifies the degree of global connectivity of the icosahedral networks would also be an interesting alternative to investigate other relevant physical processes of the MGs^[44,45].

Acknowledgment

Z.W.W. thanks the members of the “Beijing Metallic Glass Club” for the long-term fruitful discussions. This work was supported by the National Natural Science Foundation of China (Grant Nos. 52031016 and 11804027). The work was carried out at National Supercomputer Center in Tianjin, and the calculations were performed on Tianhe new generation supercomputer.

References

- [1] Wang W H 2019 Prog. Mater. Sci. **106** 100561 ISSN 0079-6425 URL <https://www.sciencedirect.com/science/article/pii/S0079642519300295>
- [2] Sheng H W, Luo W K, Alamgir F M, Bai J M and Ma E 2006 Nature **439**(7075) 419–425 URL <https://doi.org/10.1038/nature04421>
- [3] Cheng Y Q, Ma E and Sheng H W 2009 Phys. Rev. Lett. **102**(24) 245501 URL <https://link.aps.org/doi/10.1103/PhysRevLett.102.245501>
- [4] Pauly S, Gorantla S, Wang G, Kühn U and Eckert J 2010 Nat. Mater. **9**(6) 473–477 URL <https://doi.org/10.1038/nmat2767>
- [5] Inoue A 2000 Acta Mater. **48** 279–306 ISSN 1359-6454 URL <https://www.sciencedirect.com/science/article/pii/S1359645400001444>
- [6] Wang Q, Liu C T, Yang Y, Dong Y D and Lu J 2011 Phys. Rev. Lett. **106**(21) 215505 URL <https://link.aps.org/doi/10.1103/PhysRevLett.106.215505>
- [7] Liu X, Chen G, Hou H, Hui X, Yao K, Lu Z and Liu C 2008 Acta Mater. **56** 2760–2769 ISSN 1359-6454 URL <https://www.sciencedirect.com/science/article/pii/S1359645408001444>
- [8] Wang X L, Almer J, Liu C T, Wang Y D, Zhao J K, Stoica A D, Haeffner D R and Wang W H 2003 Phys. Rev. Lett. **91**(26) 265501 URL <https://link.aps.org/doi/10.1103/PhysRevLett.91.265501>
- [9] Luo W K, Sheng H W, Alamgir F M, Bai J M, He J H and Ma E 2004 Phys. Rev. Lett. **92**(14) 145502 URL <https://link.aps.org/doi/10.1103/PhysRevLett.92.145502>

- [10] Chen G L, Liu X J, Hui X D, Hou H Y, Yao K F, Liu C T and Wadsworth J 2006 Appl. Phys. Lett. **88** 203115 ISSN 0003-6951 (*Preprint* https://pubs.aip.org/aip/apl/article-pdf/doi/10.1063/1.2198015/14660781/203115_1_online.pdf) URL <https://doi.org/10.1063/1.2198015>
- [11] Martin I, Ohkubo T, Ohnuma M, Deconihout B and Hono K 2004 Acta Mater. **52** 4427–4435 ISSN 1359-6454 URL <https://www.sciencedirect.com/science/article/pii/S1359645404003118>
- [12] Della Valle R G, Gazzillo D, Frattini R and Pastore G 1994 Phys. Rev. B **49**(18) 12625–12632 URL <https://link.aps.org/doi/10.1103/PhysRevB.49.12625>
- [13] Kelton K F, Lee G W, Gangopadhyay A K, Hyers R W, Rathz T J, Rogers J R, Robinson M B and Robinson D S 2003 Phys. Rev. Lett. **90**(19) 195504 URL <https://link.aps.org/doi/10.1103/PhysRevLett.90.195504>
- [14] Cheng Y and Ma E 2011 Prog. Mater. Sci. **56** 379–473 ISSN 0079-6425 URL <https://www.sciencedirect.com/science/article/pii/S0079642510000691>
- [15] Li M, Wang C Z, Hao S G, Kramer M J and Ho K M 2009 Phys. Rev. B **80**(18) 184201 URL <https://link.aps.org/doi/10.1103/PhysRevB.80.184201>
- [16] Wu Z W, Li M Z, Wang W H, Song W J and Liu K X 2013 J. Chem. Phys. **138** 074502 ISSN 0021-9606 (*Preprint* https://pubs.aip.org/aip/jcp/article-pdf/doi/10.1063/1.4792067/14047051/074502_1_online.pdf) URL <https://doi.org/10.1063/1.4792067>
- [17] Jiang S Q, Wu Z W and Li M Z 2016 J. Chem. Phys. **144** 154502 ISSN 0021-9606 (*Preprint* https://pubs.aip.org/aip/jcp/article-pdf/doi/10.1063/1.4946866/15511205/154502_1_online.pdf) URL <https://doi.org/10.1063/1.4946866>
- [18] Mokshin A V and Barrat J L 2008 Phys. Rev. E **77**(2) 021505 URL <https://link.aps.org/doi/10.1103/PhysRevE.77.021505>
- [19] Mokshin A V and Barrat J L 2010 Phys. Rev. E **82**(2) 021505 URL <https://link.aps.org/doi/10.1103/PhysRevE.82.021505>
- [20] Wu Y, Xu B, Sun Y and Guan P 2021 Chin. Phys. B **30** 57103 URL https://cpb.iphy.ac.cn/EN/abstract/article_123471.shtml
- [21] Cui S, Liu H and Peng H 2022 Chin. Phys. B **31** 86108 URL https://cpb.iphy.ac.cn/EN/abstract/article_124977.shtml
- [22] Liu K X, Liu W D, Wang J T, Yan H H, Li X J, Huang Y J, Wei X S and Shen J 2008 Appl. Phys. Lett. **93** 081918 ISSN 0003-6951 (*Preprint* https://pubs.aip.org/aip/apl/article-pdf/doi/10.1063/1.2976667/13708787/081918_1_online.pdf) URL <https://doi.org/10.1063/1.2976667>
- [23] Gao J A, Huang H S and Lv Y J 2021 Chin. Phys. B **30** 66301 URL https://cpb.iphy.ac.cn/EN/abstract/article_123575.shtml

- [24] Ye L M, Wu Z W, Liu K X, Tang X Z and Xiong X M 2016 Chin. Phys. B **25** 068104 URL https://cpb.iphy.ac.cn/EN/abstract/article_118688.shtml
- [25] Chen S Y, Wu Z W and Liu K X 2014 Chin. Phys. B **23** 066802 URL <https://dx.doi.org/10.1088/1674-1056/23/6/066802>
- [26] Cheng Y Q and Ma E 2008 Appl. Phys. Lett. **93** 051910 ISSN 0003-6951 (*Preprint* https://pubs.aip.org/aip/apl/article-pdf/doi/10.1063/1.2966154/14400695/051910_1_online.pdf) URL <https://doi.org/10.1063/1.2966154>
- [27] Wu Z W, Li M Z, Wang W H and Liu K X 2013 Phys. Rev. B **88**(5) 054202 URL <https://link.aps.org/doi/10.1103/PhysRevB.88.054202>
- [28] Li M Z, Peng H L, Hu Y C, Li F X, Zhang H P and Wang W H 2017 Chin. Phys. B **26** 016104 URL https://cpb.iphy.ac.cn/EN/abstract/article_119282.shtml
- [29] Qiao Q, Wang J, Cai Z, Feng S, Song Z, Huo B, Li Z and Wang L M 2023 Chin. Phys. B **32** 116401 URL https://cpb.iphy.ac.cn/EN/abstract/article_126217.shtml
- [30] Peng H L, Li M Z and Wang W H 2011 Phys. Rev. Lett. **106**(13) 135503 URL <https://link.aps.org/doi/10.1103/PhysRevLett.106.135503>
- [31] Plimpton S 1995 J. Comput. Phys. **117** 1–19 ISSN 0021-9991 URL <https://www.sciencedirect.com/science/article/pii/S002199918571039X>
- [32] Zhou X W, Johnson R A and Wadley H N G 2004 Phys. Rev. B **69**(14) 144113 URL <https://link.aps.org/doi/10.1103/PhysRevB.69.144113>
- [33] Yang L, Xia J H, Wang Q, Dong C, Chen L Y, Ou X, Liu J F, Jiang J Z, Klementiev K, Saksl K, Franz H, Schneider J R and Gerward L 2006 Appl. Phys. Lett. **88** 241913 ISSN 0003-6951 (*Preprint* https://pubs.aip.org/aip/apl/article-pdf/doi/10.1063/1.2213020/13179151/241913_1_online.pdf) URL <https://doi.org/10.1063/1.2213020>
- [34] Mendelev M I, Sordelet D J and Kramer M J 2007 J. Appl. Phys. **102** 043501 ISSN 0021-8979 (*Preprint* https://pubs.aip.org/aip/jap/article-pdf/doi/10.1063/1.2769157/14865432/043501_1_online.pdf) URL <https://doi.org/10.1063/1.2769157>
- [35] Finney J L and Bernal J D 1970 Proc. R. Soc. A: Math. Phys. Eng. Sci. **319** 479–493 (*Preprint* <https://royalsocietypublishing.org/doi/pdf/10.1098/rspa.1970.0189>) URL <https://royalsocietypublishing.org/doi/abs/10.1098/rspa.1970.0189>
- [36] Borodin V A 1999 Phil. Mag. A **79** 1887–1907 (*Preprint* <https://doi.org/10.1080/01418619908210398>) URL <https://doi.org/10.1080/01418619908210398>
- [37] Schroers J, Busch R, Masuhr A and Johnson W L 1999 Appl. Phys. Lett. **74** 2806–2808 ISSN 0003-6951 (*Preprint* https://pubs.aip.org/aip/apl/article-pdf/74/19/2806/7809734/2806_1_online.pdf) URL <https://doi.org/10.1063/1.124020>

- [38] Schroers J, Johnson W L and Busch R 2000 Appl. Phys. Lett. **77** 1158–1160 ISSN 0003-6951
(*Preprint* https://pubs.aip.org/aip/apl/article-pdf/77/8/1158/7816107/1158_1_online.pdf)
URL <https://doi.org/10.1063/1.1289033>
- [39] Pauly S, Liu G, Gorantla S, Wang G, Kühn U, Kim D and Eckert J 2010 Acta Mater. **58** 4883–4890 ISSN 1359-6454 URL <https://www.sciencedirect.com/science/article/pii/S1359645410003010>
- [40] Wu Z, Li F, Huo C, Li M, Wang W and Liu K 2016 Sci. Rep. **6** 35967 URL <https://doi.org/10.1038/srep35967>
- [41] Sun G, Giovambattista N, Wang E and Xu L 2013 Soft Matter **9**(47) 11374–11382 URL <http://dx.doi.org/10.1039/C3SM52206G>
- [42] Desgranges C and Delhommelle J 2018 Phys. Rev. Lett. **120**(11) 115701 URL <https://link.aps.org/doi/10.1103/PhysRevLett.120.115701>
- [43] Desgranges C and Delhommelle J 2019 Phys. Rev. Lett. **123**(19) 195701 URL <https://link.aps.org/doi/10.1103/PhysRevLett.123.195701>
- [44] Li F X and Li M Z 2017 J. Appl. Phys. **122** 225103 ISSN 0021-8979 (*Preprint* https://pubs.aip.org/aip/jap/article-pdf/doi/10.1063/1.5004262/15205851/225103_1_online.pdf)
URL <https://doi.org/10.1063/1.5004262>
- [45] Wu Z W, Kob W, Wang W H and Xu L 2018 Nat. Commun. **9**(1) 5334 URL <https://doi.org/10.1038/s41467-018-07759-w>